The rise of a gas bubble in a viscous liquid

By D. W. MOORE
Department of Mathematics, University of Bristol

(Received 21 November 1958)

The rise of a gas bubble in a viscous liquid at high Reynolds number is investigated, it being shown that in this case the irrotational solution for the flow past the bubble gives a uniform approximation to the velocity field. The drag force experienced by the bubble is calculated on this hypothesis and the drag coefficent is found to be $32/R$, where R is the Reynolds number (based on diameter) of the bubbles rising motion. This result is shown to be in fair agreement with experiment.

The theory is extended to non-spherical bubbles and the relation of the resulting theory, which enables both bubble shape and velocity of rise to be predicted, to experiment is discussed.

Finally, an inviscid model of the spherical cap bubble involving separated flow is considered.

1. Introduction

A large number of investigations of the motion of gas bubbles in liquids have been published during the last fifty years.* The experimental method adopted is, essentially, to release a volume of gas at the bottom of a deep tank of liquid and then, when steady conditions have been attained, to determine the terminal velocity, the bubble shape and the bubble trajectory. The bubble volume V, and hence the other quantities involved, will depend on the hydrostatic pressure experienced by the bubble, so that measurements are carried out over a vertical range of distance sufficiently small for the change in hydrostatic pressure to be much less than the pressure of the gas inside the bubble.

For given gas and liquid, V or, more conveniently, the equivalent spherical radius r_e, defined by

$$\tfrac{4}{3}\pi r_e^3 = V, \tag{1.1}$$

is the only quantity at the experimenter's disposal and it is thus the aim of the experiments to relate the bubble shape, trajectory and terminal velocity to r_e and to the properties of the gas and liquid. Thus an ancillary question facing the experimenter is to determine which properties of the gas and liquid enter into this relation. Now an obvious set of properties in terms of which one can attempt to interpret the experimental data consists of the densities of the gas and liquid, ρ' and ρ; the viscosities μ' and μ; the interfacial stress T and the acceleration due to gravity g. However, the number of properties to be considered can be reduced

* The paper of Haberman & Morton (1953) gives a bibliography of the experimental literature.

if it is assumed that the motion of the enclosed gas has a negligible effect on the flow. Since the pressure and viscous stress forces exerted by the gas on the interface bear to the corresponding forces arising from the liquid motion the ratios ρ'/ρ and μ'/μ, respectively, which are small for gas-liquid bubbles [$O(10^{-3})$ and $O(10^{-2})$ for air–water] this assumption seems reasonable and will be adopted throughout this paper.

The remaining physical parameters can be combined with each other to form the dimensionless ratio M, defined by

$$M = g\mu^4/\rho T^3. \tag{1.2}$$

M is thus a property of the liquid only, and variations in M are principally due to the factor μ^4, since ρ and T do not vary much from liquid to liquid.

In addition, one can form the dimensionless Reynolds number

$$R = 2r_e U\rho/\mu, \tag{1.3}$$

and Weber number

$$W = 2r_e U^2\rho/T, \tag{1.4}$$

where U is the terminal velocity. Their dependence on U means that they are essentially unknowns, but they have the merit of possessing direct dynamical significance. In particular, W measures the ratio of the hydrodynamic pressure forces to the surface tension forces which are maintaining the shape of the bubble. If the pressure forces are weak, so that W is small, the bubble shape is determined by the condition that the surface energy is a minimum, so that the bubble is spherical. Thus one can anticipate that increasing departures of the bubble shape from the spherical will be associated with increasing values of W.

Having introduced the fundamental physical quantities which it is hoped will prove sufficient for the description of the flow, one is in a position to consider the experimental evidence. This will be taken from the experiments of Haberman & Morton (1953). These experiments were remarkable for the number of liquids used and the range of bubble sizes considered.

The experimental data on the terminal velocity, the bubble shape and the bubble trajectory will now be described. The form of the results depend in each case on the value M has for the particular liquid.

For low M liquids ($M < 10^{-8}$) the terminal velocity at first increases rapidly as r_e increases, achieves a maximum and after falling to a minimum rises gradually again. For high M liquids ($M > 10^{-3}$), the terminal velocity increases steadily with r_e, though the rate of increase falls off at a fairly well defined value of r_e.

For low M liquids the shape is at first spherical, then increasingly oblate, then, at about the radius corresponding to the maximum velocity, the shape fluctuates rapidly about an oblate form until, for very large values of r_e, the bubbles attain a striking umbrella shape which is quite steady at its frontal surface though the rear of the bubble fluctuates. These 'spherical cap' bubbles were the subject of an important investigation by Davies & Taylor (1950). For high M liquids the spherical cap shape is achieved without the bubble surface ever becoming unsteady.

For low M liquids the bubble trajectory is at first rectilinear, then, at about the bubble radius for maximum terminal velocity, both planar zig-zag and spiral

trajectories are observed. Finally, the spherical cap bubbles rise in very nearly linear trajectories. For low M liquids only rectilinear trajectories are observed.

From a dynamical point of view it is more illuminating to consider the drag coefficient C_D rather than U, and to plot it against R and W rather than r_e.

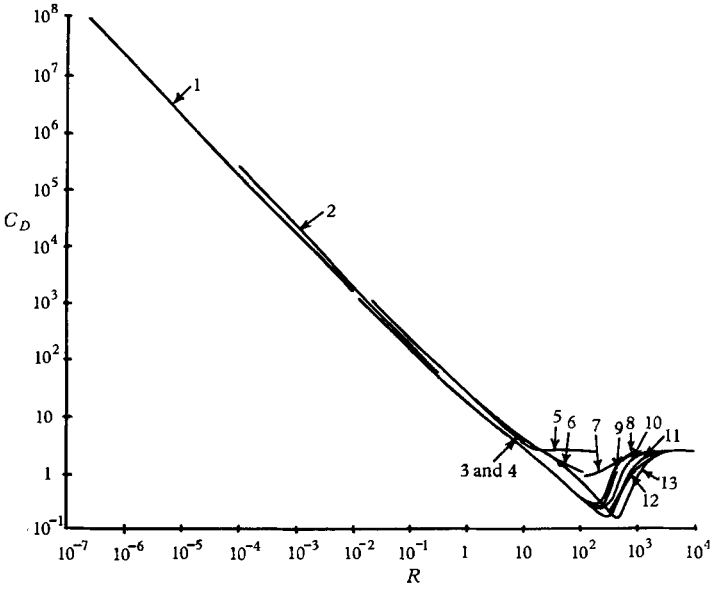

FIGURE 1. The drag coefficient as a function of the Reynolds number (reproduced from Haberman & Morton 1953).

1. Syrup (Bond), $M = 0{\cdot}92 \times 10^{6}$.
2. Olive oil (Arnold), $M = 0{\cdot}716 \times 10^{-2}$.
3. Water + 62 % corn syrup, $M = 0{\cdot}155 \times 10^{-3}$.
4. Water + 68 % corn syrup, $M = 0{\cdot}212 \times 10^{-2}$.
5. Mineral oil, $M = 1{\cdot}45 \times 10^{-2}$.
6. Water + 56 % glycerine (Bryn), $M = 1{\cdot}75 \times 10^{-7}$.
7. Water + 42 % glycerine (Bryn), $M = 4{\cdot}18 \times 10^{-8}$.
8. Turpentine, $M = 24{\cdot}1 \times 10^{-10}$.
9. Water + 13 % ethyl alcohol (Bryn), $M = 1{\cdot}17 \times 10^{-8}$.
10. Varsol, $M = 4{\cdot}3 \times 10^{-10}$.
11. Cold water (filtered), $M = 1{\cdot}08 \times 10^{-10}$.
12. Methyl alcohol, $M = 0{\cdot}89 \times 10^{-10}$.
13. Water (filtered), $M = 0{\cdot}26 \times 10^{-10}$.

C_D is determined by the condition that for steady rise the buoyancy force experienced by the bubble must balance the hydrodynamic drag force; thus

$$\tfrac{1}{2}\rho U^2 \pi r_e^2 C_D = \tfrac{4}{3} r_e^3 \rho g. \tag{1.5}$$

The results, reproduced from Haberman & Morton's paper are shown in figure 1 and figure 2. The curves in the C_D–R plane have a nearly universal form for large and small values of R, the drag coefficient having the value 2·6 for large R. The dependence on M is mainly in the range $R = O(10^2)$. On the other hand, the curves in the C_D–W plane vary greatly with M, but seem to be geometrically similar whilst having displacements parallel to the C_D axis which depend on M.

The variations are not completely systematic with respect to M, but there is a tendency for C_D to increase as M increases, for given R or W. The absence of completely systematic dependence on M suggests that too few physical parameters have been used, but whether this points to internal circulation or to some other process is not known.

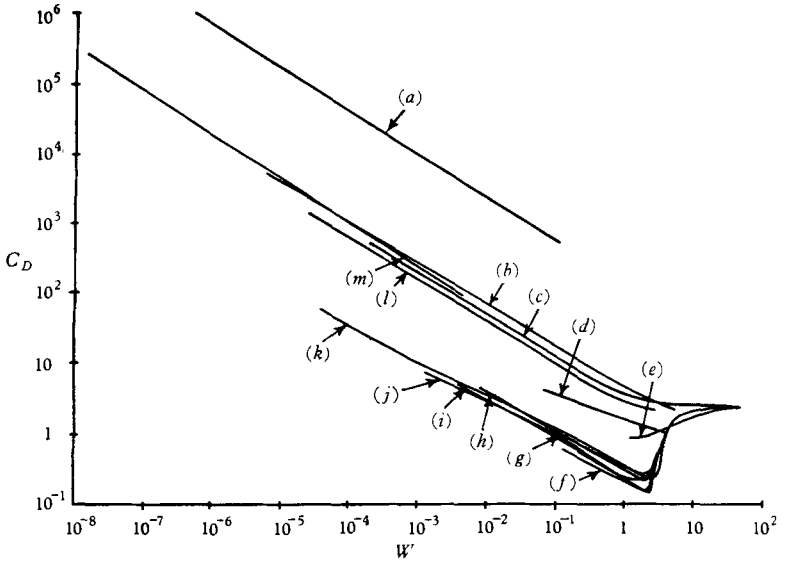

FIGURE 2. The drag coefficient as a function of the Weber number (reproduced from Haberman & Morton 1953).

(*a*) Syrup (Bond), $M = 0{\cdot}92 \times 10^{6}$.
(*b*) Water + 68 % corn syrup, $M = 0{\cdot}212 \times 10^{-2}$.
(*c*) Mineral oil, $M = 1{\cdot}45 \times 10^{-2}$.
(*d*) Water + 56 % glycerine (Bryn), $M = 1{\cdot}75 \times 10^{-7}$.
(*e*) Water + 42 % glycerine (Bryn), $M = 4{\cdot}18 \times 10^{-8}$.
(*f*) Methyl alcohol, $M = 0{\cdot}89 \times 10^{-10}$.
(*g*) Water + 13 % ethyl alcohol, $M = 1{\cdot}17 \times 10^{-8}$.
(*h*) Turpentine, $M = 24{\cdot}1 \times 10^{-10}$.
(*i*) Varsol, $M = 4{\cdot}3 \times 10^{-10}$.
(*j*) Water (filtered), $M = 0{\cdot}26 \times 10^{-10}$.
(*k*) Cold water, $M = 1{\cdot}08 \times 10^{-10}$.
(*l*) Water + 62 % corn syrup, $M = 0{\cdot}155 \times 10^{-3}$.
(*m*) Olive oil (Arnold), $M = 0{\cdot}716 \times 10^{-2}$.

The most striking feature of the curves is the very sharp minimum displayed by the drag coefficient for the low M liquids which takes place in the Reynolds number range 200–400 and the Weber number range 2–3. It is this minimum which is responsible for the maximum in the U *vs* r_e curves for low M liquids.

Thus for the low M liquids there seems to be a critical region in which the drag coefficient increases rapidly, the bubble surface ceases to be steady and the bubble trajectory ceases to be rectilinear. These effects have engaged the attention of several authors, but there has been disagreement as to their cause.

Haberman & Morton suggest that the effects are due to the onset of eddy shedding, since this is observed for rigid spheres for comparable Reynolds

numbers. Whilst the resulting appearance of periodic pressures might explain the fluctuations in the surface and the non-rectilinear form of the trajectory, the marked increases in C_D is not accounted for. More decisive evidence against their explanation is the fact that, according to Hartunian & Sears (1957), no wake exists for pure, low M liquids. Hartunian & Sears believe that instability of the bubble wall, rather than the onset of hydrodynamic instabilities in the external flow, is responsible for the effects. They point out in support of their view that the explanation in terms of hydrodynamic instability requires the effects to start in all fluids at the same critical Reynolds number, whilst their explanation implies a critical Weber number. An examination of the data points to the existence of a critical Weber number for the pure, low M liquids. They go on to consider the problem theoretically, assuming irrotational flow about a spherical bubble, and obtain a critical Weber number in good agreement with experiment. Hartunian & Sears's observations and the success of their calculations suggest that the irrotational solution is, at high Reynolds numbers, a good approximation to the actual viscous flow around a gas bubble.

This approximation is examined briefly in §2 of the present paper and it is shown to be dynamically reasonable. It is suggested that the irrotational solution forms a spatially uniformly valid approximation to the actual velocity field as the Reynolds number tends to infinity, although the stress field is not everywhere approximated by the irrotational solution. However, it is shown that, despite this restriction, the drag force on the bubble, which arises from the *normal* viscous stresses, can none the less be calculated and the result

$$C_D = 32/R \tag{1.6}$$

is obtained and shown to be in fair agreement with experiment.

§3 is devoted to the non-spherical bubble. It is shown that the shape of the bubble is determined, at high Reynolds numbers, by the pressure forces. However, even with this simplification, the determination of the bubble shape is difficult so that, following previous authors, it is assumed that the bubble is oblate ellipsoidal. The drag on the bubble is again calculated from the irrotational flow and there results an expression for C_D as a function of W and M. In particular, the theory predicts that $C_D M^{-\frac{1}{6}}$ should be a function of W only. These results are compared with experiment and the agreement is shown to be fair. The theoretical drag curve has a minimum at $W = 2{\cdot}2$ and it is suggested that this accounts for the observed minimum (though not for the subsequent sharp rise) in the experimental drag coefficient curve.

Finally, in §4 some tentative ideas on the flow around the very large spherical cap bubbles are put forward. The possibility that an inviscid model of the flow involving separation might account for the properties of the bubble is investigated.

2. The drag coefficient for a spherical bubble

In attempting to calculate the drag force experienced by a gas bubble one is at once faced with the difficulty that the bubble shape is unknown. Now it has been observed that very small air bubbles in liquids ($r_e < 0{\cdot}5$ mm in water) are spherical and, whilst these small bubbles rise relatively slowly, the Reynolds

numbers associated with the rising motion can still be large. Thus in this section the bubble will be regarded as spherical* and to emphasize this restriction the radius will be denoted by a rather than r_e.

Let the bubble be rising with constant velocity $\mathbf{U}$ in an unbounded viscous liquid at rest at infinity. Then if $\mathbf{r}$ is the position vector and $\mathbf{u}$ the fluid velocity relative to the centre of the sphere, the Navier–Stokes equations and boundary conditions are

$$(\mathbf{u}.\nabla)\,\mathbf{u} = g - 1/\rho\,\nabla p + \nu\nabla^2\mathbf{u}, \tag{2.1}$$

$$\nabla.\mathbf{u} = 0, \tag{2.2}$$

$$\mathbf{u} \to \mathbf{U} \quad \text{as} \quad |r| \to \infty, \tag{2.3}$$

$$\mathbf{u}.\mathbf{n} = 0 \quad \text{on} \quad |\mathbf{r}| = a \tag{2.4}$$

and

$$p_{n\theta} = 0 \quad \text{on} \quad |\mathbf{r}| = a, \tag{2.5}$$

where $\mathbf{n}$ is the unit outward normal at the surface of the sphere and θ is the angle between $\mathbf{r}$ and the upstream axis of symmetry.

The irrotational solution of (2.2), (2.3) and (2.4) is given by

$$\mathbf{u}_I = \nabla\left|\mathbf{U}.\mathbf{r}\left(1+\frac{a^3}{2r^3}\right)\right|, \tag{2.6}$$

and the corresponding pressure p_I is determined from (2.1) which is equivalent to Bernouilli's equation in this case, since the velocity field is irrotational. p_I is not constant on the surface of the bubble, but in view of the predominance of surface tension forces in the case of the spherical bubble this boundary condition can be ignored. The tangential stress $p_{n\theta}$ can be calculated from (2.6) and one finds that

$$p_{n\theta} = -3(\mu U/a)\sin\theta. \tag{2.7}$$

Equation (2.7) shows that (2.6) does not satisfy the boundary condition (2.5) and so cannot be the solution of the problem. However, one can modify the problem by replacing (2.5) by the boundary condition

$$p_{n\theta} = -3(\mu U/a)\sin\theta \quad \text{on} \quad |r| = a; \tag{2.8}$$

that is to say one introduces a fictitious tangential stress† distribution at the bubble surface. Then (2.6) is the exact solution of the modified problem. Furthermore, (2.8) shows that the ratio of these fictitious stresses to the inertia and pressure forces tends to zero as $\mu \to 0$ for fixed a and $\mathbf{U}$. Thus it is plausible to assume that when the Reynolds number R is large, the irrotational solution provides a uniformly valid approximation to the inertia forces and hence to the velocity field. Clearly, the velocity gradient or stress field will not be everywhere derivable from (2.6), since the small fictitious stresses are never zero and there will thus be a region adjoining the bubble surface in which the relative error in the stress field is $O(1)$. However, this does not contradict the assertion that the inertia forces are uniformly approximated by those of the irrotational solution, since normal gradients occur in the inertia terms multiplied by the normal velocity component and this vanishes at the bubble surface. The author has shown

* This is equivalent to assuming that the Weber number is very small.

† The device of invoking fictitious external forces to render an approximate solution exact was suggested by Lamb's (1932, p. 609) discussion of the Stoke's approximation.

elsewhere (Moore 1958) that this region has the character of a boundary layer in which tangential stress, though not the tangential velocity, has an $O(1)$ difference from the values predicted by (2.6).

It must be pointed out that R cannot be made large without limit since, as was noted in § 1, there exists for each liquid a critical Reynolds number at which a change in nature of the flow takes place. However, this critical Reynolds number is itself large (> 200), so that there exists a range of subcritical Reynolds numbers in which it is reasonable to apply the approximation just described.

The equation of continuity for axial flow is, in spherical polar co-ordinates,

$$\frac{\partial u}{\partial r}+\frac{2u}{r}+\frac{1}{r\sin\theta}\frac{\partial}{\partial\theta}(v\sin\theta)=0, \tag{2.9}$$

where u and v are the components of the velocity along and perpendicular to the radius vector. Now the considerations of the preceding paragraphs suggest that the irrotational solution (2.6) furnishes, at large Reynolds numbers, a uniform approximation to the velocity field (u, v) so that $v(r, \theta)$ and $\partial v/\partial\theta$ are derivable from the irrotational solution. Equation (2.9) thus shows that the normal rate of change of the normal velocity component is also uniformly approximated by the irrotational solution, despite the fact that $\partial v/\partial r$ is not approximated by the irrotational solution. It is this property of the approximation which enables the drag force experienced by the bubble to be calculated.

The tangential stress at the bubble surface is zero and, accordingly, the drag force arises entirely from the normal viscous stresses. Now, in spherical polar co-ordinates,

$$p_{rr}=-p+2\mu\frac{\partial u}{\partial r}, \tag{2.10}$$

where p is the pressure. Thus, using the irrotational solution (2.6), one finds that

$$p_{rr}=-p_I-6(\mu U/a)\cos\theta. \tag{2.11}$$

The drag force D is now easily calculated and one finds that

$$D=8\pi\mu Ua, \tag{2.12}$$

so that the drag coefficient for a spherical bubble is given by

$$C_D=32/R. \tag{2.13}$$

This is the main result of the present paper. It is subject to the restrictions that R is to be large (but subcritical) and that W has to be small. That these two conditions are not mutually exclusive follows from the observed occurrence of spherical bubbles at large Reynolds numbers. A relation between R and W is derived in the next section and this also predicts that both conditions can be satisfied in low M liquids.

A comparison of (2.13) with some experimental measurements of drag coefficients is shown in figure 3. Points were selected from the curves given by Haberman & Morton for spherical bubbles in varsol and 13 % ethyl-alcohol + water mixture. Evidently (2.13) is in fair agreement with experiment, although the theoretical drag coefficient seems to be somewhat too small.*

* Dr Saffman suggested to the author that this might be due to a small amount of form drag caused by separation of the boundary layer.

If, as is suggested in this paper, the irrotational solution furnishes, at high Reynolds numbers, a uniformly valid approximation to the velocity field, it is clear that the wake behind the bubble must be of a rather weak character, in the sense that the velocities in the wake region differ only slightly from those of the irrotational solution. This does not mean that the wake is of no dynamical importance—indeed the momentum loss due to the velocity defect in the wake must be equal to the rate of working of the drag force acting on the bubble and,

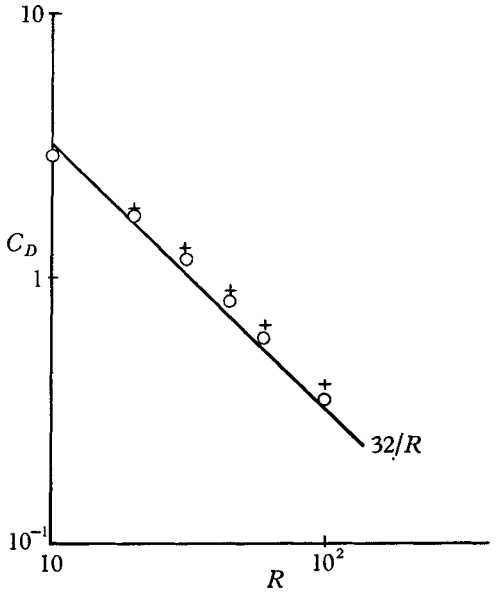

FIGURE 3. The theoretical drag coefficient for spherical bubbles compared with representative points from Haberman & Morton's (1953) experimental curves. +, 13 % ethyl alcohol + water; ○, varsol.

also, the wake region makes a significant contribution to the total viscous dissipation—but it does imply that the wake is not likely to be easily observable. Hartunian & Sears's observations, referred to in § 1, suggest that there is no wake behind gas bubbles in pure, low M liquids although wakes of an unusual, apparently closed form are observed behind bubbles in impure liquids.

3. The non-spherical bubble

The photographs given by Haberman & Morton show that the rectilinearly rising bubble can achieve quite considerable departures from the spherical. Hartunian & Sears (1957) estimated, from this photographic data, that the bubble diameter perpendicular to the trajectory could be as great as twice the diameter parallel to the trajectory. Thus the question arises of whether or not the above calculation can be extended to cover the non-spherical bubble or, in other words, whether or not the restriction $W \ll 1$ can be removed. The problem of determining the drag coefficient is now considerably complicated by the fact that the bubble shape is also unknown and has to be determined as part of the calculation.

Corresponding to this extra unknown is the additional boundary condition, to be satisfied at every point of the bubble surface,

$$p_{nn} = T\left(\frac{1}{R_1}+\frac{1}{R_2}\right)+\text{const.}, \tag{3.1}$$

where R_1 and R_2 are the principal curvatures. This condition expresses the constancy of the internal gas pressure. Both viscous forces and pressure forces contribute to p_{nn}, but since the viscous stress is smaller by a factor of order $1/R$ than the pressure its contribution can be neglected and the shape of the bubble calculated as if the flow were inviscid. However, the dependence of the pressure forces on the irrotational flow and hence on the bubble shape is non-linear so that the problem of determining the bubble shape is difficult.

It is natural to start by considering the case of the nearly spherical bubble and this case was treated by Hartunian & Sears (1957). The bubble shape will be taken to be the ellipsoid of revolution

$$r = a[1+\epsilon P_2(\cos\theta)] \quad (\epsilon \ll 1). \tag{3.2}$$

Then, calculating the pressure forces from the irrotational flow above a sphere, one has

$$\tfrac{9}{8}\rho U^2 \sin^2\theta + O(\epsilon\rho U^2) = 4T(\epsilon/a)\,P_2(\cos\theta) + O(T\epsilon^2/a), \tag{3.3}$$

where the approximate formula for the total curvature given by Lamb (1932, p. 474) has been used. Thus, one must have

$$\epsilon = -\tfrac{3}{16}(U^2 a\rho/T). \tag{3.4}$$

To the order of this approximation it does not matter whether the Weber number is based on a or the equivalent spherical radius r_e, so that introducing the ratio χ of the transverse and longitudinal axes of the bubble, one has

$$\chi = 1+\tfrac{9}{64}W. \tag{3.5}$$

Thus the bubble is oblate.

Some discussion of the neglected terms in (3.3) is of interest. The term $O(\epsilon\rho U^2)$ arises from the effect of the change of shape on the pressure field, whilst the term $O(\epsilon^2 T/a)$ arises from the use of the approximate formula for the total curvature. Equation (3.4) shows that these terms are in fact of the same order of magnitude. The calculation of the deformation due to Hartunian & Sears seems to be in error at this point, since they attempt to improve the linear theory by retaining only the term arising from the perturbation to the pressure field.

The result (3.5) shows that deformations from the spherical are not important if $W < \frac{1}{10}$ and one can regard this as providing an estimate of the range of validity of the expression for C_D given in §2.

One might attempt to improve the linear theory by assuming a more general shape in place of (3.2) and retaining terms of higher order in the departures from the spherical, but, in addition to the fact that such a calculation would be very lengthy, it seems unlikely that one could get a valid result for large deformations without using an inordinately large number of terms. One can instead, following Hartunian & Sears, assume that the bubble is oblate ellipsoidal for all values of the axis ratio. One cannot then satisfy the boundary condition (3.1) at all points

of the bubble surface and, indeed, it seems clear that the bubble is exactly oblate ellipsoidal only for vanishingly small values of $\chi - 1$. One can, however, insist that (3.1) be satisfied at the points of the bubble surface where the total curvature is a maximum and minimum, that is to say at the nose and at the equator. A similar assumption about the shape was made by Saffman (1956), but the approximate method of satisfying the surface pressure condition employed there was different.

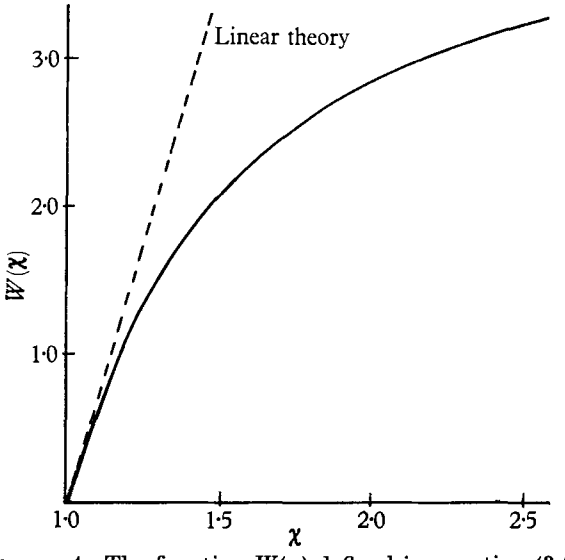

FIGURE 4. The function $W(\chi)$ defined in equation (3.6).

Now the potential flow about an oblate ellipsoid of revolution is described by Lamb (1932, p. 142) and thus the pressure force at the surface of the bubble can be calculated. The condition that (3.1) is to be satisfied at the points of maximum and minimum curvature determines W as a function of χ and one finds, after some algebra, that

$$W(\chi) = 4\chi^{-\frac{4}{3}}(\chi^3 + \chi - 2)\,[\chi^2 \sec^{-1}\chi - (\chi^2 - 1)^{\frac{1}{2}}]^2\,(\chi^2 - 1)^{-3}. \tag{3.6}$$

A similar result was obtained by Hartunian & Sears. The function $W(\chi)$ is plotted in figure 4 and it is seen that the linear theory is a good approximation for only a very limited range of values of $\chi - 1$.

When the bubble shape has been determined, it remains to calculate the drag force experienced by a bubble of this shape. The structure of the flow about the spherical bubble was such that the normal viscous stresses could be calculated from the potential flow about the sphere and it seems reasonable to expect that this would be the case for bubbles of a more general shape. Thus if the potential flow about the bubble is known the drag force can be calculated without difficulty and, again invoking the details of the potential flow about an oblate ellipsoid of revolution, one has, after a lengthy calculation,

$$C_D = (32/R)\,F(\chi), \tag{3.7}$$

where

$$F(\chi) = \frac{\chi^{\frac{4}{3}}}{2}\left[\frac{(\chi^2 - 1)^{\frac{1}{2}} - (2 - \chi^2)\sec^{-1}\chi}{\chi^2 \sec^{-1}\chi - (\chi^2 - 1)^{\frac{1}{2}}}\right]. \tag{3.8}$$

The graph of $F(\chi)$ is shown in figure 5 and it can be seen that the drag coefficient increases with increasing oblateness.

Now once C_D is known, the terminal velocity U is known, by virtue of the relation (1.5) expressing the balance of the buoyancy force and the drag force. Thus, under the assumption of oblate ellipsoidal shape, (3.6), (3.7) and (3.8) provide, since they are equivalent to two equations in the two unknowns U and χ, the complete solution of the problem of determining the terminal velocity and degree of oblateness of a bubble rising steadily at high Reynolds number. However, the exact relations between the unknowns and r_e cannot be found explicitly, owing to the complicated way in which χ enters the equations and in order to

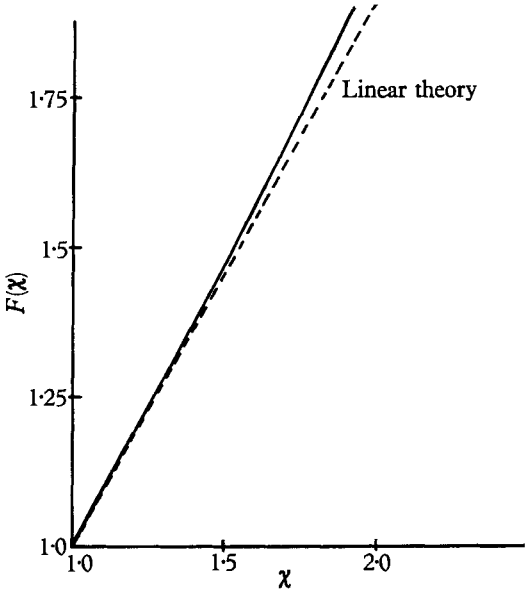

FIGURE 5. The function $F(\chi)$ defined in equation (3.8).

illustrate the nature of the results, a linear theory, arising from the expansion of R and W in powers of $\chi - 1$, will first be given. This linear theory has the additional advantage that it makes no assumption as to the bubble shape for, as has been seen, it follows rigorously from the analysis that, provided that terms of $O(\chi-1)^2$ are ignored, the bubble is an oblate ellipsoid of revolution.

The function $F(\chi)$ can be expanded in powers of $\chi - 1$ and one finds that

$$F = 1 + \tfrac{14}{15}(\chi - 1) + \ldots. \tag{3.9}$$

Now equation (1.5) yields the relation

$$U = \tfrac{1}{6} r_e^2 (\rho g/\mu)\,(F)^{-1}, \tag{3.10}$$

whereas the Reynolds number R is, by definition,

$$R = 2 r_e \rho U/\mu. \tag{3.11}$$

These equations enable r_e and U to be determined as functions of R and of the constants of the liquid, so that the Weber number can be calculated as a function of R; thus,

$$W = (3^{\frac{5}{3}}/18)\, F^{-\frac{1}{3}} R^{\frac{5}{3}} M^{\frac{1}{3}}. \tag{3.12}$$

One can now eliminate W between this equation and (3.5) and on substituting into (3.9) one has

$$C_D = 32/R\{1 + (3^{\frac{5}{3}}/240)\, R^{\frac{5}{3}} M^{\frac{1}{3}} + \ldots\}, \tag{3.13}$$

since the variation of F in (3.10) contributes only second-order terms. This expression for C_D predicts that, for the lower values of R, the drag coefficient has the universal value $32/R$ in all liquids but that as R increases, the different liquids display increasing departures from this universal form. Furthermore, for given R, C_D is an increasing function of M. Both these features are present in the curves in the C_D–R plane given by Haberman & Morton, although the variations with respect to M are not completely systematic. One can also express C_D as a function of W and, to the order of the approximation, one has

$$C_D = (6/18^{\frac{3}{5}})\, M^{\frac{1}{5}} W^{-\frac{3}{5}} + \ldots. \tag{3.14}$$

If the relation between C_D and W were displayed on log-log graph paper (3.14) would predict that the drag coefficient curves were parallel straight lines of slope $-\frac{3}{5}$. This is seen to be approximately the case from figure 2.

As was stressed in the introduction, the presentation of results about bubble motion should, from the point of view of dynamical interpretation, be in terms of the dimensionless numbers C_D, R, W and M, rather than in terms of the directly measured quantities r_e and U. However, the results of this section can readily be converted to this direct form if required. One result, in direct form, of the linear theory, is an expression for the departures from the spherical in terms of the equivalent radius. This is

$$\chi = 1 + \tfrac{1}{128} r_e^5 (\rho^3 g^2 / T\mu^2), \tag{3.15}$$

so that the axis ratio depends very strongly on the ratio of r_e to the characteristic length $T^{\frac{1}{5}}\mu^{\frac{2}{5}} g^{-\frac{2}{5}} \rho^{-\frac{3}{5}}$. For water this length is about 0·2 mm and this provides an idea of the size of bubble at which departures from the spherical will, on the above theory, become apparent.

Returning to the non-linear theory one can, formally, go through the procedure which leads to (3.14) and one finds that, without approximation,

$$C_D = (96/18^{\frac{3}{5}})\, M^{\frac{1}{5}} W^{-\frac{3}{5}} [F\{\chi(W)\}]^{\frac{4}{5}}. \tag{3.16}$$

Thus the non-linear theory predicts that $C_D/M^{\frac{1}{5}}$ should be a function of W only. However, before comparing this ratio with its experimental values, one must express the condition that R is large in terms appropriate to the C_D–W plane. In fact (3.12) shows that

$$R = W^{\frac{3}{5}} (18^{\frac{3}{5}}/3)\, F^{\frac{1}{5}} M^{-\frac{1}{5}} \tag{3.17}$$

and, since W can be of $O(1)$, one must require that

$$M^{-\frac{1}{5}} \gg 1. \tag{3.18}$$

More precisely, if a Reynolds number of 50 is regarded as the lower bound of the range of validity of the theory, then

$$M < 10^{-7}, \tag{3.19}$$

so that the theory is restricted to low M liquids.

The function $C_D/M^{\frac{1}{6}}$ as given by (3.16) is plotted in figure 6 together with values of $C_D/M^{\frac{1}{6}}$ for several low M liquids. These were taken from the experimental curves of Haberman & Morton. It is seen that the agreement is fair for several of the low M liquids for $W < 3$, although the predicted values are on the whole too low. An unexpected feature of the theoretical drag curve is the minimum at $W \doteqdot 2{\cdot}2$. It seems usually to have been assumed that the drag coefficient would be a monotonic decreasing function of W, so that the sharp minimum displayed by the experimental curves has been associated with the onset of an instability of

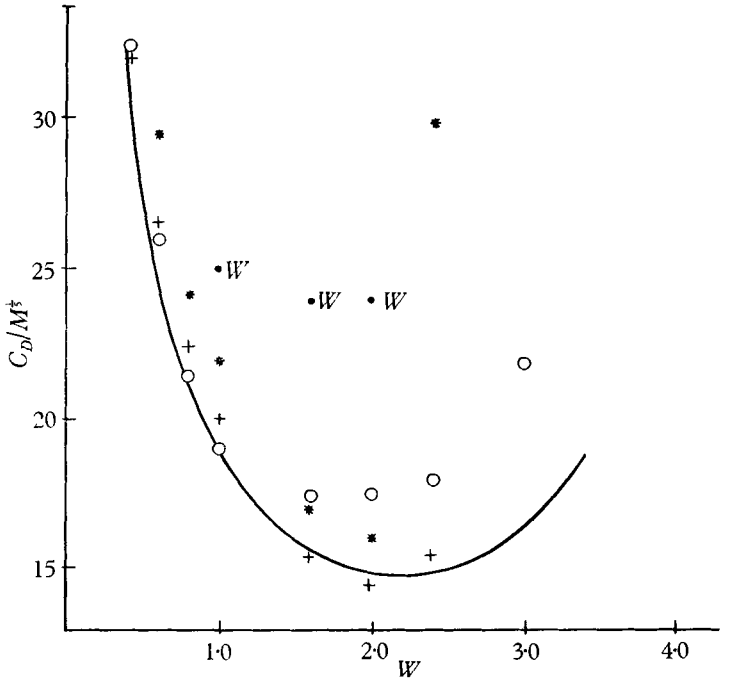

FIGURE 6. The theoretical relation between C_D and W compared with experimental values (taken from Haberman & Morton's curves) for several low M liquids. o, Varsol; +, turpentine; *, methyl alcohol; W, water.

the flow. The present work suggests, however, that the minimum is a property of the steady flow. This view is, to some extent, confirmed by a comparison of Hartunian & Sears's measurements with those of Haberman & Morton. Hartunian & Sears estimated the critical Weber number for the onset of instability by observing a large number of bubbles in the critical region and noting the size of bubble which was just large enough to oscillate. This gave a critical Weber number of 3, in good agreement with their calculations. However, it can be seen from figure 2 that the *minimum* in the experimental drag curves of Haberman & Morton are at about $W = 2$.

It must be emphasized that the theoretical drag curve ceases to be in even order of magnitude agreement with experiment for values of W much greater than 3. For example, at $W = 3{\cdot}75$, $C_D/M^{\frac{1}{6}}$ is about 28, whilst the experimental values are of $O(100)$. Evidently, some other mechanism is responsible for the

sharp increase of the drag, possibly an instability of the type investigated by Hartunian & Sears. In any case, the approximation of regarding the bubble as oblate ellipsoidal is not likely to be reliable for values of χ much greater than 2·2, which corresponds to a Weber number of 3.

The relation (3.17) between R and W is shown graphically in figure 7, so that the C_D *vs* R curve can be constructed if required. Since

$$\frac{dC_D}{dR} = \frac{dC_D}{dW}\frac{dW}{dR}, \tag{3.20}$$

it is clear that there will be a minimum in this curve at the value of R given by

$$R_{\min} = 3{\cdot}3M^{-\frac{1}{6}}. \tag{3.21}$$

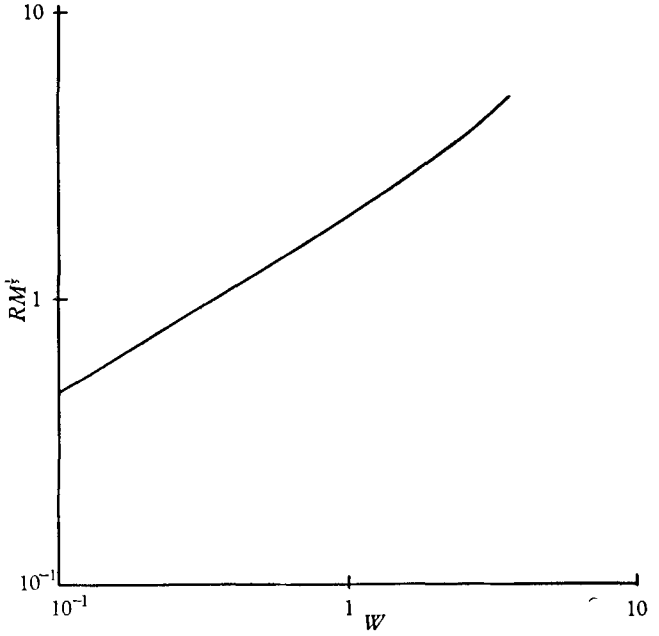

FIGURE 7. The theoretical relation between R and W as predicted by equation (3.17).

The minimum value depends on M, however, and so is different for the different liquids, as is observed experimentally. A comparison with experimental data is shown in table 1, the minima being roughly estimated from Haberman & Morton's curves.

It is clear from figure 6 that the drag coefficients for bubbles in water are considerably above the predicted values. That the behaviour of bubbles in water is, to some extent, different from that in other low M liquids, was noticed by Hartunian & Sears. They found that critically stable bubbles in water had an oblateness of about 1·5, whilst in most other liquids the value was 2·1. It is well known that it is extremely difficult to purify water, so that it is natural to seek an explanation of this discrepancy in terms of impurities. Haberman & Morton conducted tests in which surface active substances were added to the water used in bubble experiments and found that as little as $\frac{1}{2}$ % of the substance caused the

drag coefficient to rise to the value for a rigid sphere. They suggest that the molecules of the surface active substance collect at the surface of the bubble which thus behaves as a rigid body as far as the hydrodynamic boundary conditions are concerned. This idea is supported by Hartunian & Sears's observation of a critical Reynolds number in 'dirty' liquids and the fact that such bubbles can possess a wake. With these observations in mind, it is not unreasonable to suggest that

Liquid	Observed $R_{\min}$	Calculated $R_{\min}$
Water + 42 % glycerine	100*	95
Water + 13 % ethyl alcohol	200	130
Turpentine	170	175
Varsol	230	245
Cold water (filtered)	300	325
Methyl alcohol	300	335
Water (filtered)	450	430

* Existence of minimum not certain.

TABLE 1

the water used in Haberman & Morton's experiments contained small concentrations of impurities which were sufficient to raise the drag coefficient towards the rigid sphere value. It is significant that the use, by Hartunian & Sears, of double distilled water, reduced the discrepancy in the critical oblateness by about 50 %.

4. The spherical cap bubble

The observations of Davies & Taylor (1950) showed that very large air bubbles in nitrobenzene assumed a remarkable umbrella-like form. The curved surface was uppermost and was steady and almost exactly spherical. The rear surface was unsteady and fluctuated about the plane passing through the rim of the curved upper surface. These 'spherical cap' bubbles have been observed in other low M liquids and in high M liquids also, though in this case the rear surface was steady and nearly plane. The transition to this shape is not sudden, but seems to occur gradually as values of the Weber number of the order of twenty are approached.

Let the bubble be regarded as being at rest in a uniform stream of velocity U. The flow will be regarded as inviscid. Let R denote the radius of the spherical surface and let θ be the angle between any radius of this surface and the axis of symmetry. Then if $U(\theta)$ is the velocity at any point of the spherical surface, one must have, since the interior pressure is constant

$$\tfrac{1}{2}\rho U^2(\theta) + \rho g R\cos\theta = \rho g R \tag{4.1}$$

(in view of the large values of the Weber number characterizing this type of bubble, surface tension is ignored). If, following Davies & Taylor, one assumes that the flow near the curved surface of the bubble is identical with the potential flow about a complete sphere of the same radius, then

$$U(\theta) = \tfrac{3}{2}U\sin\theta. \tag{4.2}$$

Thus, on substituting into (4.1), one finds that

$$\tfrac{9}{8}\rho U^2 \sin^2\theta + \rho g R\cos\theta = \text{const.} \tag{4.3}$$

Clearly, this equation cannot be satisfied exactly for any choice of U, but Davies & Taylor point out that it is satisfied as far as the terms in θ^2 in the power series expansions of the trigonometric functions, so that the pressure condition is satisfied near the nose of the bubble if

$$U = \tfrac{2}{3}(gR)^{\frac{1}{2}}. \tag{4.4}$$

Davies & Taylor showed that (4.4) was in good agreement with the experimental relation between U and R. Rosenberg (1950) has verified that $U \propto (gR)^{\frac{1}{2}}$, but suggests that the coefficient should be slightly reduced to the value 0·645. Thus we may regard this relation as having been firmly established.

No further progress can be made without making some assumption as to the nature of the flow at the rear of the bubble. In particular, the shape of the bubble is unknown, so that even though the terminal velocity is given by (4.4), the drag coefficient cannot be determined.

The approximation of regarding the flow as inviscid, which is, in view of the discussion in § 2, likely to be reliable at the front of the bubble, may well break down at the rear where the relatively large value of the drag coefficient suggests that flow separation of some sort must take place. However, one might hope to account for the drag coefficient on the basis of a potential solution involving separation of the flow along a surface of discontinuity and it is the object of this section to examine this solution. The bubble will be regarded as being exactly of the spherical cap form, so that the problem of finding the bubble shape reduces to determining the angle θ_m of the cap. It will be assumed that the flow separates from the bubble at the join of the curved and plane surfaces and that the flow downstream consists of an infinite axi-symmetric wake of stagnant fluid, separated from the rest of the flow by a surface of discontinuity. This surface is clearly one of constant dynamic pressure and so of constant velocity. Thus the problem is mathematically equivalent to that of determining the shape of the axi-symmetric cavity behind a solid obstacle of the same shape as the bubble. Unfortunately, no method of solution, analogous to the well-known hodograph plane method in the two-dimensional case, is available. However, it will prove possible to determine θ_m without finding the exact shape of the cavity.

Let V be the velocity of the fluid just at the surface of discontinuity. Then since the velocity of the fluid must be continuous at the points where this surface leaves the bubble, one must have

$$V = U(\theta_m). \tag{4.5}$$

Equation (4.5) also ensures that the pressure is continuous at the plane surface of the bubble. Now, since the wake is assumed to extend to infinity, the velocity at wake boundary must be equal to the uniform velocity of the fluid at downstream infinity which is, by continuity, equal to the velocity of the fluid at upstream infinity. Thus, from (4.5),

$$U = U(\theta_m). \tag{4.6}$$

If one assumes that U is related to the radius R of the cap by (4.4), substitution into (4.1) shows that

$$\theta_m = \cos^{-1}\tfrac{7}{9} \doteqdot 39°. \tag{4.7}$$

Thus, even though no details of the wake flow have been elucidated, θ_m has been determined. However, the value is somewhat outside the range observed by Davies & Taylor, the mean value of θ_m being about 52°.

The volume V of the bubble is given in terms of R and θ_m by the relation

$$V = \pi R^3(\tfrac{1}{3}\cos^3\theta_m - \cos\theta_m + \tfrac{2}{3}) \tag{4.8}$$

so that the buoyancy force $\rho g V$ is known. Then, since U is given in terms of R by (4.4), the drag coefficient (as defined in §1; Davies & Taylor employ a different definition) can be found and one has

$$C_D \doteqdot 2{\cdot}1. \tag{4.9}$$

The experimental value is 2·6.

One can determine the asymptotic form of the wake using a result due to Levinson (1946). Levinson proved that the asymptotic relation between the radius r and the distance downstream x for the infinite axi-symmetric constant pressure cavity behind an obstacle is

$$r \sim cx(\log x)^{-\frac{1}{4}} \quad \text{as} \quad (x \to \infty), \tag{4.10}$$

where c is a constant, and that, moreover, the drag force D experienced by the obstacle responsible for the cavity is given by

$$D = \tfrac{1}{8}(\pi\rho U^2 c^2), \tag{4.11}$$

where U is the velocity of the uniform stream. Thus equating this expression for the drag to the buoyancy force $\rho g V$ and invoking (4.4) one has

$$c \doteqdot 0{\cdot}85R. \tag{4.12}$$

It is not surprising that the value of the drag coefficient predicted by this theory is somewhat too small, since the actual flow is almost certainly turbulent. Indeed, owing to an optical anisotropy of nitrobenzene, Davies & Taylor were able to observe the turbulence behind spherical cap bubbles and were even able to estimate the turbulent dissipation, which turned out to be of the same order of magnitude as the rate of working of the drag force. The actual wake was approximately spherical, the surface being quite well defined in the photograph given by Davies & Taylor. This suggests that perhaps a more realistic model would be one of the closed streamline type discussed by Batchelor (1956), although this type of wake would lead to a zero value of the drag coefficient.

What is most likely is that no satisfactory explanation of the properties of the bubble can be obtained on inviscid theory, whatever assumptions are made. However, in lieu of any more realistic theoretical approach, investigations of this type are perhaps worth making. In particular, a more general approach to the inviscid, discontinuous flow, which regarded the bubble shape also as being an unknown, would perhaps throw some light on why the bubbles adopt the curious spherical cap shape. However, the resulting boundary value problem is formidable.

The author has benefited from some interesting discussions with Dr P. G. Saffman, who drew his attention to the problems of bubble motion at high

Reynolds numbers. Dr Saffman also made some helpful comments on the first draft of this paper. During the period of preparation of this paper the author was in receipt of a maintenance allowance from the Department of Scientific and Industrial Research. The author is indebted to the Director of the David W. Taylor Model Basin for permission to reproduce figures 16 and 17 from Haberman & Morton (1953).

REFERENCES

BATCHELOR, G. K. 1956 *J. Fluid Mech.* **1**, 388.
DAVIES, R. & TAYLOR, G. I. 1950 *Proc. Roy. Soc.* A, **200**, 375.
HABERMAN, W. L. & MORTON, R. K. 1953 *David Taylor Model Basin, Rep.* no. 802.
HARTUNIAN, R. A. & SEARS, W. R. 1957 *J. Fluid Mech.* **3**, 27.
LAMB, H. 1932 *Hydrodynamics*, 6th ed. Cambridge University Press.
LEVINSON, N. 1946 *Annals of Math.* **47**, 704.
MOORE, D. W. 1958 Ph.D. Thesis, Cambridge University.
ROSENBERG, B. 1950 *David Taylor Model Basin, Rep.* no. 727.
SAFFMAN, P. G. 1956 *J. Fluid Mech.* **1**, 249.